Diffusive-to-ballistic transition in grain boundary motion studied by atomistic simulations

Chuang Deng and Christopher A. Schuh[*]

Department of Materials Science and Engineering, Massachusetts Institute of Technology, 77 Massachusetts Ave,
Cambridge, Massachusetts 02139, USA

An adapted simulation method is used to systematically study grain boundary motion at velocities and driving forces across more than five orders of magnitude. This analysis reveals that grain boundary migration can occur in two modes, depending upon the temperature (T) and applied driving force (P). At low P and T, grain boundary motion is diffusional, exhibiting the kinetics of a thermally activated system controlled by grain boundary self-diffusion. At high P and T, grain boundary migration exhibits the characteristic kinetic scaling behavior of a ballistic process. A rather broad transition range in both P and T lies between the regimes of diffusive and ballistic grain boundary motion, and is charted here in detail. The recognition and delineation of these two distinct modes of grain boundary migration also leads to the suggestion that many prior atomistic simulations might have probed a different kinetic regime of grain boundary motion (ballistic) as compared to that revealed in most experimental studies (diffusional).

PACS number(s): 61.72.Mm, 81.05.Bx, 81.07.Bc, 82.20.Wt

I. INTRODUCTION

The motion of grain boundaries (GBs) is central to the microstructural evolution in every class of polycrystalline materials, and yet a deep understanding of the kinetics of GB motion is still lacking. The challenge primarily results from the complexity of the GB structural space. There is a broad spectrum of GBs; in general, five parameters are required to describe the macroscopic structure of a GB: three for the lattice misorientation and two for the GB plane normal.[1–4] Furthermore, GB motion is relevant over a wide range of temperatures, from subambient to the melting point of the material (T_m) during thermal or mechanical processing.[5–7] The driving forces for GB motion, in addition, can also span many orders of magnitude; for curvature-driven migration alone these can span from $\sim 10^2$ Pa in coarse grained materials to as high as $\sim 10^9$ Pa when the grain sizes are reduced to several nanometers,[8] while extrinsic driving forces such as mechanical shearing, interaction with lattice defects, etc., can also be in play in some situations.[6,7,9,10] So far, only a relatively small portion of this vast parameter space has been explored in controlled experiments, including only a small number of GBs across the five-parameter GB space, under limited conditions [GB velocity: $10^{-8} \sim 10^{-3}$ m/s; driving force: $10^2 \sim 10^6$ Pa; temperature: above 0.7 T_m (see Ref. 7)]. New techniques that can access more of the relevant problem space are thus desired.

With the rapid development of high-speed computing in the last decade, atomistic simulation has emerged as an alternative method to study GB motion.[11–33] Atomistic simulation, such as molecular dynamics (MD), is not constrained from the point of view of sample preparation and allows more flexibility in adjusting the system temperature and driving force. Therefore a variety of MD techniques have been developed in recent years to study GB motion, and these can be grouped into two main categories.

The first category of MD techniques, which we term "driven motion" methods, extracts the GB mobility based on a proportionality established from empirical experimental observations:[7]

$$v = MP, \qquad (1)$$

where v is GB velocity, P is driving force, and M is the GB mobility, which follows an Arrhenius relation:

$$M = M_0 \exp\left(\frac{-Q_m}{kT}\right), \qquad (2)$$

where M_0 is a preexponential constant, k is the Boltzmann constant, T is temperature, and Q_m is the activation energy for GB migration. In this category, a variety of approaches have been developed to apply controlled driving forces, P, and two of these have been most widely used to study the motion of planar GBs. One is the "elastic deformation method,"[15,17,32–34] which involves an elastic strain applied to a bicrystal with elastic anisotropy in the two grains. The different energy changes induced in the two grains due to elastic anisotropy provides a driving force for the GB to move into the grain of higher energy and thereby lower the overall system energy. The other technique is the "synthetic driving force method,"[11,23,35] which involves the artificial addition of different amounts of energy to atoms in a bicrystal according to their local lattice orientation. A driving force arises at the GB due to the energy difference across it, similarly to the "elastic deformation method."

Both of these two methods can effectively drive a planar GB to move. However, due to the short time scale in typical MD simulations, the slowest reported GB velocity extracted from driven motion methods is ~ 1 m/s,[11,15,23,32] which is orders of magnitude higher than typical experimental measurements [($10^{-8} \sim 10^{-3}$ m/s (see Ref. 7)]. Concomitantly, the driving force used in such MD simulations is usually $\sim 10^8$ Pa,[11,15,23,32] also several orders of magnitude higher than typical experimental values [$10^2 \sim 10^6$ Pa (see Ref. 7)]. Such discrepancies make it difficult to directly compare results from experiments and MD simulations. As a corollary, the reported activation energies for GB motion obtained by these techniques are often significantly lower than experimentally measured values.[15,23,32]

The second category of techniques, the "fluctuating boundary" techniques, in contrast, require no external driving force; the mobility of a GB is extracted from the interface

thermal fluctuations. Currently two different methods have been developed in this category. The first method, developed by Foiles and Hoyt,[36] applies to rough interfaces and generally not to highly symmetric GBs, while the second, so-called "interface-random-walk method"[31] developed by Trautt *et al.*, is more general. However, the major limitation for either method is that very high temperatures, usually above about 0.80 T_m, are required in order to obtain measurable interface fluctuations over the MD time scale.[31] And there is another drawback; although this method can be used to extract GB mobilities in the zero-velocity limit, it is not applicable in investigating the kinetics of grain boundary motion, e.g., how GB velocity scales with the driving force. Unusually low activation energies, e.g., ~0.3 eV for Ni, have also been predicted with this technique due to the limitations of the accessible temperature range.

Since all existing methods to simulate grain boundary motion have their weaknesses, we have proposed in a recent preliminary report a new approach that can significantly extend the scope of accessible regimes of GB motion without increasing the computing demand.[37] The new approach is based on the adaptation of existing MD methods from both "driven motion" and fluctuating boundary techniques. In particular, an adaptation of the interface-random-walk method was developed by enhancing the sampling statistics of GB motion caused by thermal noise. As a result, subtle interface fluctuations at temperatures as low as ~0.2 T_m can be measured. Moreover, we demonstrated that this method can be extended to study slow GB motion at net velocities as low as ~10^{-4} m/s, by synergizing the boundary fluctuation analysis with an applied bias. We refer to the resulting technique as the adapted interface random walk (AIRwalk) method.[37]

In this paper, we apply the AIRwalk method of Ref. 37 to study GB motion at driving forces and velocities spanning a very broad range—more than five orders of magnitude. This permits a detailed discussion of the kinds of GB motion that may be seen under various circumstances, and, in particular, allows us to identify separate kinetic regimes that have not been previously clearly delineated. These developments help to unify the current view of GB kinetics, and bring together the seemingly disparate pictures offered by prior experiments and MD simulations.

II. METHODS

A. Adapted interface-random-walk method

The interface-random-walk method described in Ref. 31 was initially proposed to extract GB mobility at net zero driving force and zero normal GB velocity. This method is based on the fact that when exposed to a given temperature, a large number (l) of GBs of identical geometry but different initial conditions should deviate from their original positions [$h_j(0)$, $j = 1, 2, \ldots, l$] randomly; that is to say, statistically, the average position among these l GBs at any specific time t should remain unchanged [$\langle h_j(t) - h_j(0) \rangle = 0$, here $\langle \ldots \rangle$ denotes the ensemble average for $j = 1, 2, \ldots, l$), while the variance {$\langle d_j^2(t) \rangle = \langle [h_j(t) - h_j(0)]^2 \rangle$} linearly increases with

time according to

$$D = \frac{\langle d_j^2(t) \rangle}{t} = \frac{2MkT}{A}, \quad (3)$$

where D is a boundary "diffusion" coefficient and A is the interface area.

This technique was extended in Ref. 37 to study GB motion under a small driving force by recognizing that the stochastic nature of GB motion due to thermal noise should persist under bias. We term the technique involving a nonzero driving force as the "adapted interface-random-walk method." Since the AIRwalk method was only sketched in broad strokes in Ref. 37, we present some further details on the methodology here.

First, we redefine the GB diffusion coefficient D. The original definition of D in Eq. (3) implies that the variance of GB displacement $\langle d_j^2(t) \rangle$ linearly increases from zero with time ($\langle d_j^2(0) \rangle = D \times 0 = 0$). As shown in Fig. 1, if in each simulation the GB displacement is measured after every time interval of $\Delta t = t_{i+1} - t_i$, $i = 0, 1, 2, \ldots, n$, the underlying assumption of Eq. (3)[31] is that the GB displacements $d_j(\Delta t_i)$ and $d_j(\Delta t_{i'})$ during any given time intervals Δt_i and $\Delta t_{i'}$ are uncorrelated to each other as long as $i \neq i'$. However, this assumption is not valid for adjacent time intervals when $i' = i + 1$, since the end position and final velocity of the GB during time interval t_i are always the starting position and
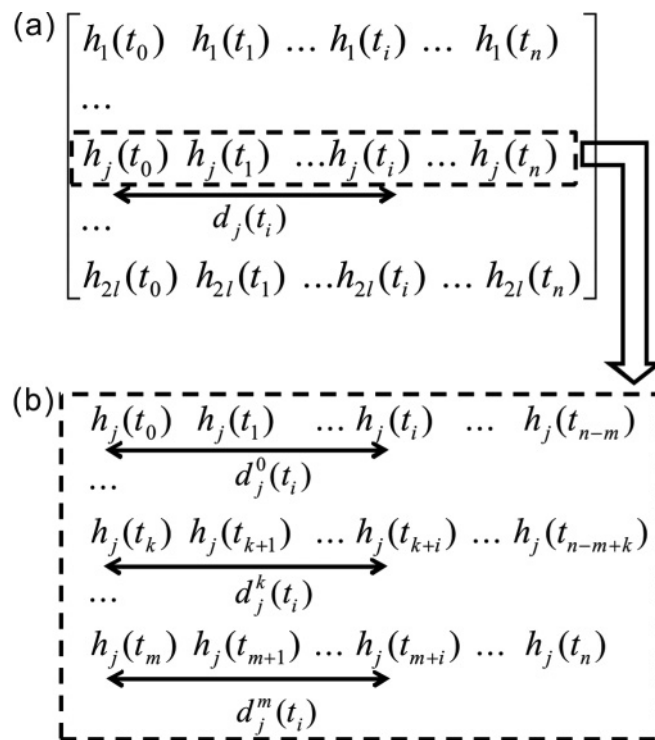
FIG. 1. Schematic showing the measurement of grain boundary displacement $d_j(t_i)$ by the (a) original interface-random-walk method[31] and (b) adapted-interface-random-walk method. In (a), each row denotes a series of measurements of position at different times, t, for a given simulated boundary; there are $2l$ rows corresponding to the two boundaries in each of the l simulation cells. In (b), each row is expanded to reflect increased sampling of many different time intervals in a given simulation, inflating the number of viable data points.

initial velocity of the GB during time interval t_{i+1}. Therefore, at time $t = t_n$ one can write

$$\langle d_j^2(t_n)\rangle = \langle[d_j(\Delta t_1)+d_j(\Delta t_2)+\cdots+d_j(\Delta t_{n-1})+d_j(\Delta t_n)]^2\rangle$$
$$= n\langle d_j^2(\Delta t)\rangle + 2(n-1)\langle d(\Delta t_i)d(\Delta t_{i'})\rangle, \qquad (4)$$

where the cross term $\langle d(\Delta t_i)d(\Delta t_{i'})\rangle$ is nonzero only when $i' = i + 1$, $i \leqslant n - 1$. From Eq. (4), we derive that

$$\langle d_j^2(t)\rangle = \frac{t}{\Delta t}\big[\langle d_j^2(\Delta t)\rangle + 2\langle d_j(\Delta t_i)d_j(\Delta t_{i+1})\rangle\big]$$
$$\qquad - 2\langle d_j(\Delta t_i)d_j(\Delta t_{i+1})\rangle,$$
$$= Dt - C_0 \qquad (5)$$

with the diffusion coefficient D redefined as

$$D = \frac{d\langle d_j^2(t)\rangle}{dt} = \frac{1}{\Delta t}[\langle d^2(\Delta t)\rangle + 2\langle d(\Delta t_i)d(\Delta t_{i+1})\rangle], \quad (6)$$

and $C_0 = 2\langle d(\Delta t_i)d(\Delta t_{i+1})\rangle$, which converges to a constant value as time increases.

Second, we inflate the effective sample size N by several orders of magnitude, not by performing more simulations, but by recognizing that Eq. (6) should remain unchanged no matter what the initial condition is. As shown in Fig. 1, for l independent simulations, we can immediately inflate the number of GB displacements $d_j(t_i)$ at any time interval of $t_i = i\Delta t$ from $N = 2l$ (each simulation cell contains two independent GBs, as shown in Fig. 2) as defined from a single, fixed initial position $h_j(t_0)$ in the original interface-random-walk method,[31] to $N = 2l(m + 1)$ by redefining $d_j(t_i)$ as

$$d_j^k(t_i) = h_j(t_{k+i}) - h_j(t_k),$$
$$j = 1,2,\ldots l, \quad k = 0,1,2,\ldots,m, \qquad (7)$$
$$i = 1,2,\ldots n - m, \quad m < n.$$

The third adaptation we introduce to the method from Ref. 31 is that for any time interval of $t_i = i\Delta t$ we fit the $N = 2l(m + 1)$ data points of GB displacement $d(t_i)$ from Eq. (7) to a cumulative distribution function as in Eq. (8):

$$F(x) = \frac{1}{2}\left[1 + \mathrm{erf}\left(\frac{x - \mu}{\sigma\sqrt{2}}\right)\right], \qquad (8)$$

where $F(x)$ is the probability that $d_j(t_i)$ falls in the interval $(-\infty, x]$, erf is the error function, and $\mu = \langle d_j^k(t_i)\rangle$, $\sigma^2 = \langle d_j^k(t_i)^2\rangle$ are the expected value and variance of the GB displacement $d_j(t_i)$. Equation (8) is obtained by integrating the expected Gaussian distribution of $d_j(t_i)$ into a cumulative form, and fitting the full data set to this equation has accuracy advantages over simply averaging. For instance, if the mean value of $d_j(t_i)$ were calculated as the straight ensemble average among the $N = 2l(m + 1)$ data points instead, we would have

$$\langle d_j^k(t_i)\rangle = \frac{1}{2l(m+1)}\sum_j\sum_k d_j^k(t_i)$$
$$= \frac{1}{2l(m+1)}\sum_j\sum_k h_j(t_{k+i}) - h_j(t_k),$$
$$j = 1,2,\ldots,2l; \quad k = 0,1,2,\ldots,m;$$
$$i = 1,2,\ldots,n - m; \quad m < n. \qquad (9)$$
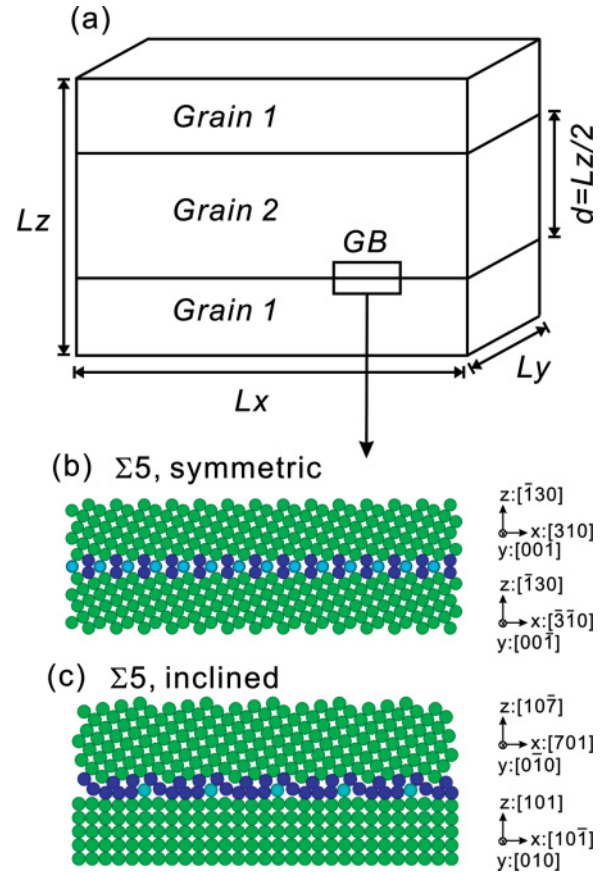
FIG. 2. (Color online) (a) Schematic of the simulation cell with periodic boundary conditions applied along x, y, and z directions; the atomistic configuration and plane indices of the (b) symmetric and (c) inclined $\Sigma 5$ grain boundaries. Atom colors correspond to local lattice structures.

Setting $i = 1$ for demonstration purposes, Eq. (9) becomes

$$\langle d_j^k(t_1)\rangle = \frac{1}{2l(m+1)}\sum_j h_j(t_{m+1}) - h_j(t_0),$$
$$j = 1,2,\ldots,2l; \quad m < n. \qquad (10)$$

Equation (10) clearly shows that in each simulation only the data points at $t = t_0$ and $t = t_{m+1}$ (total data points $N = 2l$) have been used, and the majority of information at time intervals in between has been discarded. In contrast, every data point [total data points $N = 2l(m + 1)$] can be used by fitting to Eq. (8).

B. GB geometry and simulation setup

As shown in the schematic of Fig. 2(a), each simulation cell contains two GBs, with periodic boundary conditions imposed along all three axes. Two types of GBs have been studied; both are Ni $\Sigma 5$ $\langle 100\rangle$ tilt GBs, but with different GB plane inclinations, one of which is termed "symmetric" and one "inclined." The atomistic configurations including the plane indices of both types of GBs are shown in Figs. 2(b) and 2(c), respectively. The atom colors correspond to the local crystal structure according to Ackland-Jones analysis.[38] This analysis method is also used to track the GB position when no

bias is applied, defined by the sites with non-fcc coordination. The simulation cell dimensions $\{L_x, L_y, L_z\}$ are $\{17.8, 1.0, 22.3 \text{ nm}\}$ (symmetric) and $\{10.0, 1.4, 21.7 \text{ nm}\}$ (inclined), respectively.

MD simulations are performed using the software package LAMMPS[39,40] with embedded atom method potentials developed for Ni[40] using an isothermal, isobaric (constant number of atoms N, pressure P, and temperature T with Nose-Hoover thermostat[41,42]) ensemble. This particular potential is used in order to be consistent with our previous study, where we confirm that similar mechanistic results are produced with a second potential for Ni. [37] The time step is set to be 5 fs. The simulation cell is relaxed by using a "heating-and-quenching" approach.[43,44] Specifically, each system is first relaxed at 1300 K and P = 0 for 25 ps, followed by a gradual annealing to the desired temperature in 25 ps, and subsequently relaxed at the desired temperature for another 25 ps prior to the simulation. For simulations in which a bias is applied, a force is exerted upon atoms near the GB according to the method developed by Janssens *et al.*.[23] Specifically, a certain amount of artificial energy (in eV) is added to each atom depending on the local lattice orientation: zero for atoms at perfect lattice sites in one grain, Δe for atoms at perfect lattice sites in the other grain, and some value between zero and Δe for atoms close to the GB. The normal GB velocity can thus be calculated by tracking the change of the total amount of artificially added energy ΔE, such that

$$v = \frac{1}{2} \frac{d[\Delta E(t)/\Delta e]}{dt} \frac{l_z}{N_{\text{total}}}. \tag{11}$$

Here, l_z is the dimension of the simulation cell normal to the GB plane, N_{total} is the total number of atoms in the simulation cell, and the factor of two is introduced because the change of $\Delta E(t)$ is due to the motion of two identical GBs moving towards (or away from) each other. Δe is set as an input to exert the desired driving force ($P = \Delta e 1.6 \times 10^{-19} \text{ Pa}/V_{\text{atom}} = \Delta e 1.6 \times 10^{-19} \text{ Pa}/(a^3/4) \sim \Delta e 1.47 \times 10^{10} \text{ Pa}$ for Ni, here V_{atom} is the atomic volume of Ni, and $a = 0.352$ nm is the lattice constant). The number of independent simulations, the duration of each simulation, and the analysis method depend on the magnitude of the GB velocity. Usually, one simulation of up to 500-ps duration is used if $v > 1$ m/s, 12 simulations of 1-ns duration are used if $v < 1$ m/s, and the use of the AIRwalk method and Eq. (8) becomes critical when $v < 0.1$ m/s. In all simulations, the GB position is calculated every 0.5 ps.

III. RESULTS

A. GB velocity measurement

An example showing the measurement of GB velocity via Eq. (11) is given in Fig. 3, which shows the time variance of the total amount of artificially added energy, $\Delta E(t)$, in the simulation cell with inclined Ni $\Sigma 5$ GBs at different temperatures. The applied bias is $\Delta e = 0.05$ eV per atom ($\sim$0.735 GPa) at the interfaces. Regardless of the temperature, ΔE linearly decreases as a function of time, which is consistent with a constant GB velocity. Introducing the values for each parameter in Eq. (11), e.g., $\Delta e = 0.05$ eV, $N_{\text{total}} = 27584$, $l_z = 21.7$ nm, the GB velocities can be calculated as 6.1 (600 K), 37.5 (800 K), 65.6 (1000 K), and 89.5 m/s (1200 K),
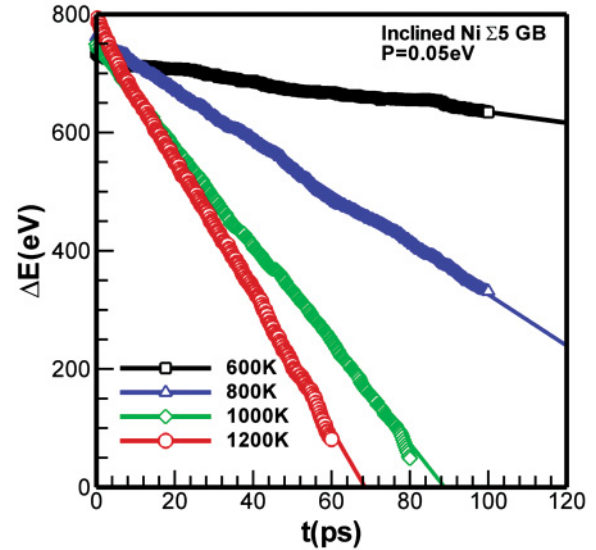
FIG. 3. (Color online) Evolution of the total amount of artificially added energy that drives boundary motion, during the migration of inclined Ni $\Sigma 5$ grain boundaries at various temperatures.

respectively. The uncertainty on these measurements is quite small, being estimated as $\pm 2\%$.

B. Dependence of *v* on *P*

We have simulated the motion of GBs at velocities and driving forces spanning more than five orders of magnitude, e.g., v $\sim 10^{-3}$–10^2 m/s and P $\sim 10^5$–10^9 Pa (equivalent to $\Delta e \sim 10^{-5}$–10^{-1} eV), as shown in Figs. 4(a) and 4(d), for the symmetric and inclined $\Sigma 5$ boundaries respectively. At the highest temperatures we studied, the data appear linear, i.e., GB velocity scales linearly with driving force, in line with Eq. (1). However, from these figures, it is immediately observed that for most of the investigated temperatures the GB velocity increases quite nonlinearly with the applied driving force for both types of GBs, which is contrary to the generally assumed linear trend as described in Eq. (1). The nonlinearity is generally more evident at lower temperatures, and can be seen with even more clarity by examining the double-logarithmic representations of the same data in Figs. 4(b) and 4(e).

In fact, the log-log presentations in Figs. 4(b) and 4(e) suggest that multiple regimes of behavior may exist, depending on the driving force. Specifically, we find that there are two apparently linear regimes with a transition in between. This is most clearly observed by examining the intermediate temperatures on the log-log scales, i.e., $T < 1000$ K in Figs. 4(b) and 4(e). In these conditions, the data exhibit an s-shaped curve that transitions from a slope of unity to one much higher, then back to unity, as P increases. The transitions of slope are better represented in Figs. 4(c) and 4(f) by plotting the derivatives at each data point on Figs. 4(b) and 4(e). The two tails of the curves are convincingly linear regimes, with $(P/v)(dv/dP) \sim 1$, separated by a steeper slope in between. The first linear regime occurs when the applied bias is high, which is quite clearly seen in Figs. 4(a) and 4(d), e.g., when $P > 0.05$ eV at $T > 700$ K for both types of
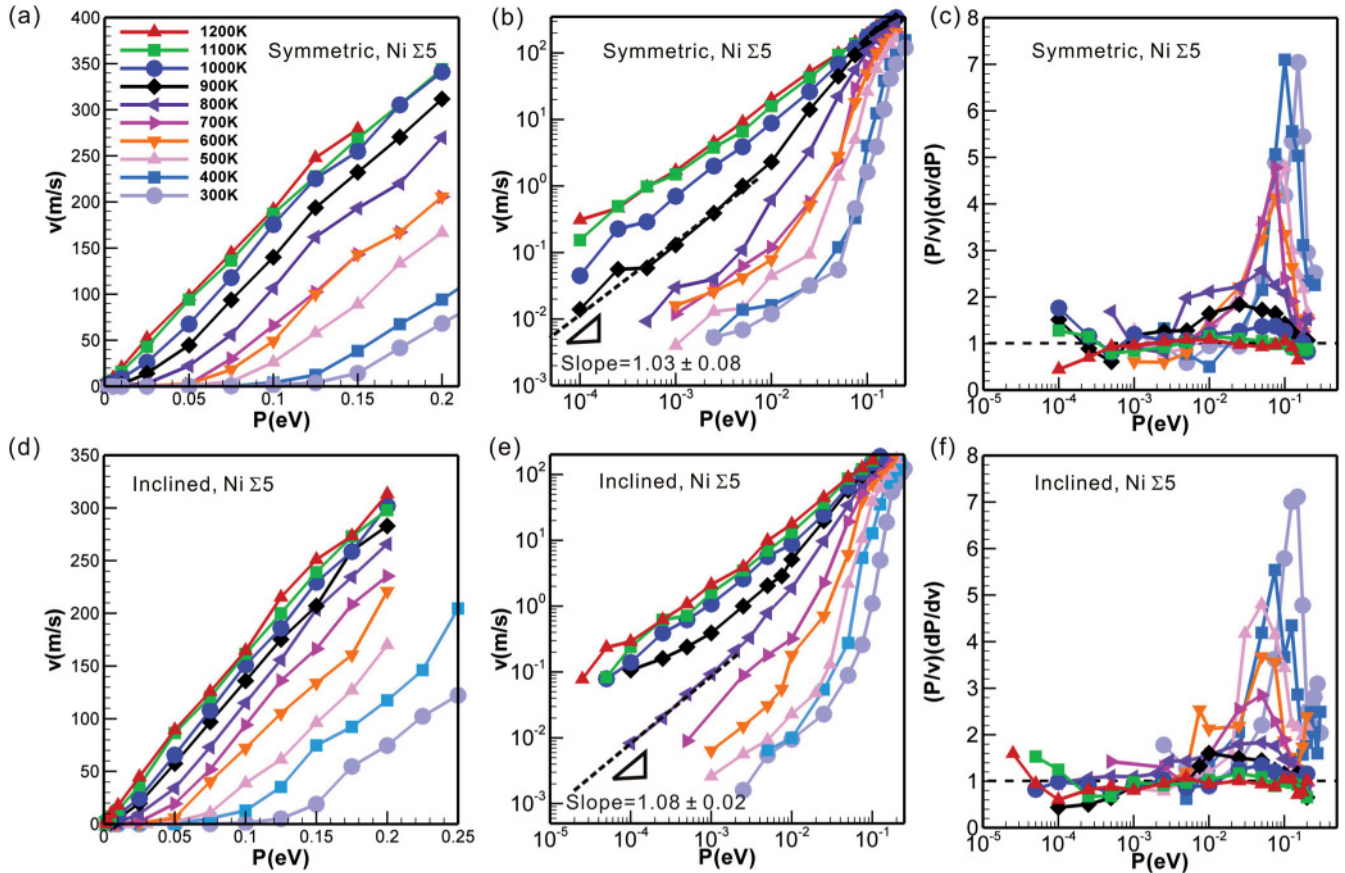
FIG. 4. (Color online) The boundary velocity v vs driving force P at various temperatures for the (a) symmetric and (d) inclined Ni $\Sigma 5$ grain boundaries; v vs P at various temperatures in the log-log scale for the (b) symmetric and (e) inclined Ni $\Sigma 5$ grain boundary; the slope value at each data point on the log-log plot for the (c) symmetric and (f) inclined Ni $\Sigma 5$ grain boundary. Here, the driving force can be converted to Pa according to 1eV $\sim 1.47 \times 10^{10}$ Pa.

GBs. The second linear regime, in contrast, is when the bias is sufficiently small, as shown in the log-log plot of Figs. 4(b) and 4(e), e.g., when $P < 0.005$ eV at $T > 700$ K for both GBs. The transition between the two apparent linear regimes is more abrupt and occurs at higher biases when the temperature is lower [see Figs. 4(c) and 4(f)]; the transition is subtle at high temperatures, e.g., $T > 1000$ K, or even unnoticeable at $T = 1200$ K.

IV. DISCUSSION

Our delineation of two different kinetic regimes of GB motion, each of which exhibits a linear bias-velocity relationship, and each of which is dominant in different ranges of temperature and bias, represents the key result of this work. A map, demarcating these regimes, is shown in Fig. 5, which summarizes the results presented in Fig. 4. In this map, the shading corresponds to the slope values $(P/v)(dP/dv)$ as in Figs. 4(c) and 4(f). Specifically, the symbols in blue color represent the two linear regimes with a slope value close to unity, which are separated by a transition area enclosed by the dashed lines. The Figs. 5(a) and 5(b) show that the details of the transition are somewhat dependent upon the structure of the boundary, with the transition being somewhat wider for the

symmetric boundary. Nonetheless, all of our data speak to two distinct modes of GB migration, separated in the P-T space.

We believe these two regimes correspond to different modes of GB motion that are reminiscent of the low-bias "diffusional" and high-bias "ballistic" kinetic regimes seen for other driven kinetic processes. We are inspired by prior work on such processes, such as for biased diffusion on crystalline surfaces, studied as the Brownian motion of particles in a tilted washboard potential.[45,46] For such processes, when the external bias P is sufficiently small, the particles are "locked," i.e., oscillate around their equilibrium positions with occasional thermally activated random jumps over the energy barrier back and forth, migrating with a net velocity of $v \propto \exp(P/kT)$, which can be reduced to a simple linear relation $v \propto P$ when P is small ($P/kT \ll 1$). In contrast, the particles move essentially ballistically, in the "running" state, when the external force is very large; in this case too, the displacement of the particles is linear with time.[45,46] When the external force P is in the intermediate range, sufficiently large but below that required to trigger the stable running state motion, dynamic transitions between locked and running states occur, which lead to an intermediate velocity averaging the two modes.[45,46]

This kind of diffusional-ballistic mode transition is exactly in line with our observations of GB motion in Fig. 4. If indeed GB motion can be described as either locked or running in
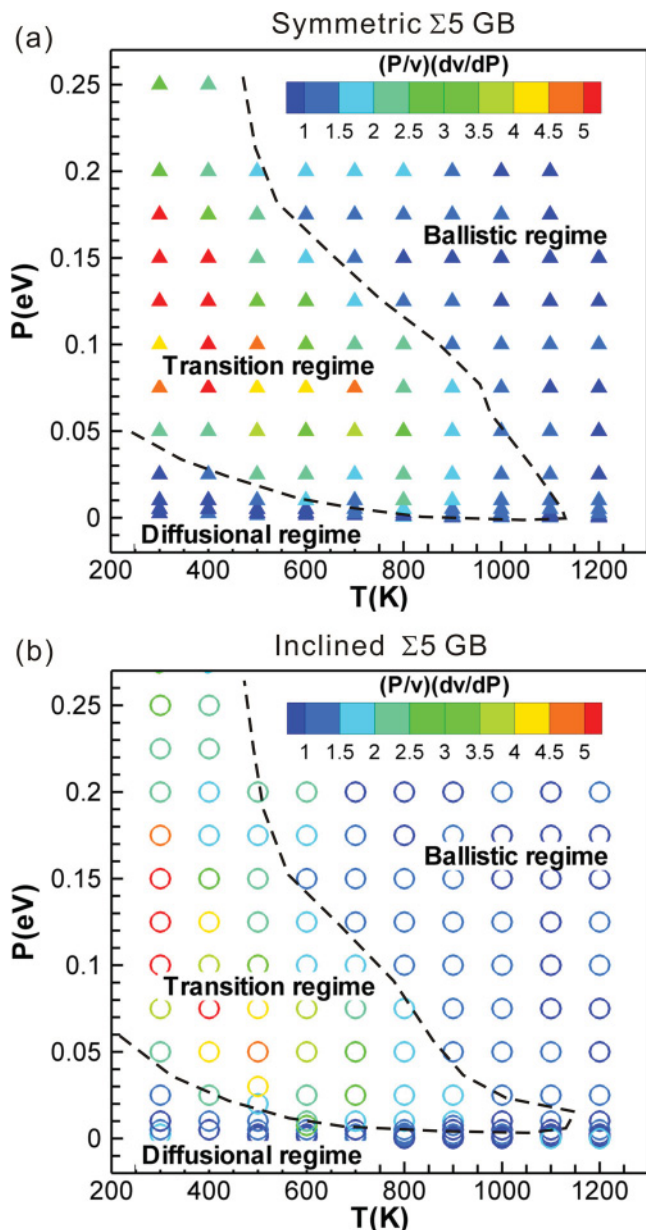
FIG. 5. (Color online) A map of the modes of GB migration, built using the local slope value of $\ln v$ vs $\ln P$ at various temperatures and driving forces for the (a) symmetric and (b) inclined Ni $\Sigma 5$ grain boundaries. The dashed lines separate diffusional, transition, and ballistic regimes of grain boundary motion. Here, the driving force can be converted to Pa according to $1 \text{eV} \sim 1.47 \times 10^{10}$ Pa.

this sense, then there are several expectations that emerge. First, at low driving forces, the locked state should exhibit the characteristics of a diffusional system, e.g., stochastic behavior that is dominated by thermal effects. Second, at higher driving forces, we should observe behavior that comprises some combination of locked/diffusional activity as well as periods of running motion. Finally, at sufficiently high driving forces, ballistic or running state activity as for free particles should emerge and eventually dominate the GB motion. In the following, we will identify the diffusional/locked and ballistic/running states in GB motion and investigate how the transitions between them occur. Finally, the influence of

applied driving force on the measured activation energy of GB migration is discussed.

A. GB motion in the locked or diffusional state

It is expected from the above discussion that GB motion should exhibit diffusional characteristics in the locked state (at low driving forces). For GB migration, the natural diffusional process to anticipate is, literally, a thermally activated mass diffusion process in the GB (i.e., GB self-diffusion). While experimental studies have often revealed comparable activation energies for processes of GB migration and GB diffusion,[7,47–49] MD simulations based on driven motion methods[15,17,23,32] have consistently reported significantly lower activation energies for GB migration than diffusion, usually by a factor of $3 \sim 5$.[15,17,32] Such discrepancies have sometimes been attributed to the presumed existence of impurities in experimental studies that might have significantly lowered the GB mobility.[15,17,32] However, MD studies directly comparing GB migration and diffusion in pure metals with no possibility of impurity effects bear out the discrepancy: GB migration studied by the driven motion methods yield an extracted activation energy for GB migration that is still significantly lower than that for simulated GB self-diffusion in the identical MD structure.[32]

We believe that the very high GB velocities involved in past MD simulations[15,17,23,32] may underlie the discrepancy between results reported for GB migration and self-diffusion. In our recent preliminary report on the AIRwalk method,[31] we proposed that GB motion in the low-velocity regime (net velocity ~ 0 m/s) is indeed achieved via diffusion, which we inferred from our measured activation energies for GB migration closely matching those for GB diffusion measured experimentally; although experimental work on GB migration of the exact same geometry is not available, the typical experimental values of activation energy are in line with our simulated results. With the addition of the new data in Fig. 4, we are now able to further articulate our conjecture: we believe that the low-driving force mode of GB motion is diffusional, while the high-P mechanism is not; driven MD simulations probe a different mode of GB motion that is not diffusional, and thus produce an apparent discrepancy as compared to experiments that probe the diffusional mechanism.

In order to further confirm our conjecture, we now proceed to develop a direct comparison between GB migration and diffusion. To do so, we simulate GB self-diffusion by tracking the mean square displacement of GB atoms for both symmetric and inclined $\Sigma 5$ GBs, following the procedure of Liu *et al.*[50] and Suzuki *et al.*.[51] GB atoms are defined as those in a 1 nm-wide slab containing the GB, and their displacements are measured as a function of time under no bias to assess self-diffusion in the boundary.

Figure 6(a) shows a few example datasets for the displacement of GB atoms in the inclined $\Sigma 5$ GB; the atomic displacement increases linearly with time at all temperatures. The GB self-diffusivity is defined as[50,51]

$$D_{\text{GBS}} = D_0 \exp\left(\frac{-Q_D}{kT}\right)$$
$$= \frac{\sum \left[(x_i - x_{i0})^2 + (y_i - y_{i0})^2 + (z_i - z_{i0})^2\right]}{6 N_{\text{GB}} t}, \quad (12)$$
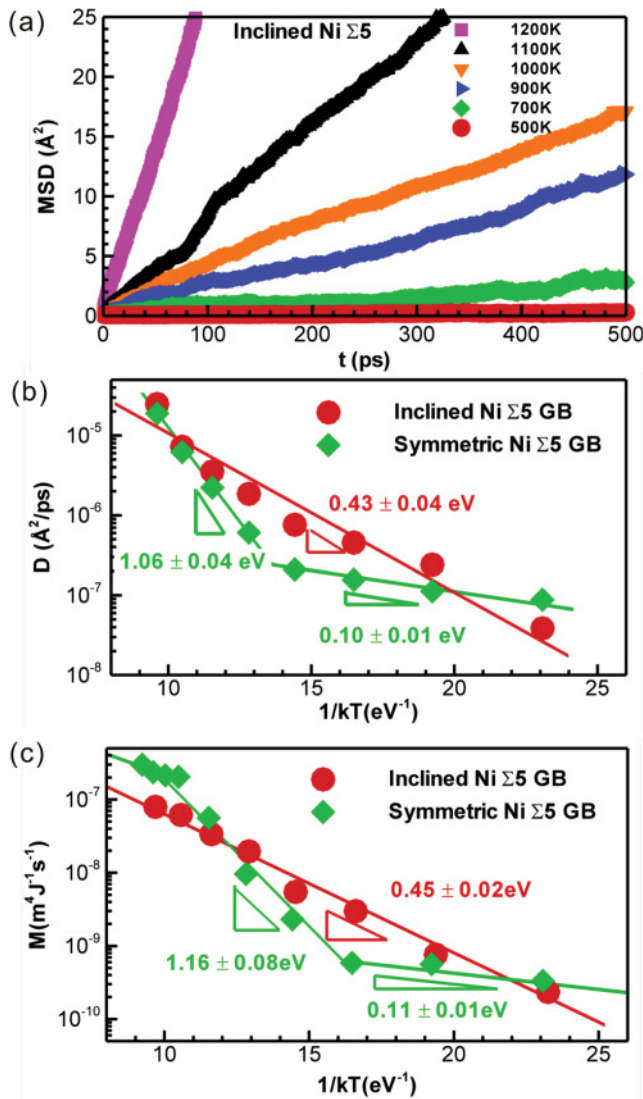
FIG. 6. (Color online) (a) The evolution of mean square displacement of grain boundary atoms in the inclined Ni Σ5 grain boundary at various temperatures; the Arrhenius plot of (b) the self-diffusivity and (c) mobility for both symmetric and inclined Ni Σ5 grain boundaries. The activation energies extracted from the slope of linear fittings are also indicated.

where Q_D is the activation energy for GB self-diffusion, x_i, y_i, z_i are the coordinates of GB atom i ($i = 1, 2, ..., N_{GB}$) at time t, and x_{i0}, y_{i0}, z_{i0} are the initial coordinates of atom i, N_{GB} is the total number of GB atoms in the slab. Note that the diffusion coefficient D used in Eq. (3) is different from the self-diffusivity D_{GBS} calculated according to Eq. (12): D is a kinetic descriptor of the boundary motion kinetics, while D_{GBS} characterizes atomic diffusion in the grain boundary.

The resulting GB diffusivities are presented in the Arrhenius plot of Fig. 6(b). In this figure, we see a significant effect of the GB plane upon the diffusion kinetics and mechanism in the studied temperature range (500–1200 K); whereas the inclined boundary exhibits a single regime with an intermediate activation energy of 0.43 eV, the symmetric boundary shows a more complex transition of behaviors, including a low-temperature regime with a low activation energy of 0.10 eV, and a high-temperature regime with a high activation energy of 1.06 eV. This interesting behavior for the symmetric Σ5 GB can be attributed to a transition of the diffusional mechanisms; prior simulation work has shown[50] that the GB diffusional process is dominated by interstitials when the temperature is relatively low and by vacancies when it is high.

More interesting than the diffusion measurements themselves is their comparison to the kinetics of GB migration. Figure 6 shows a comparable Arrhenius plot of our measurements of GB mobility at zero driving force ($P = 0$). Examining this figure in light of the diffusion data in Fig. 6(b), it is clear that for both types of GBs, the activation energy for GB migration agrees very well with that for GB self-diffusion, e.g., $Q_m = 0.45 \pm 0.02$ eV in comparison with $Q_D = 0.43 \pm 0.04$ eV in the inclined Ni Σ5 GB, and $Q_{m1} = 1.16 \pm 0.08$ eV, $Q_{m2} = 0.11 \pm 0.01$ eV in comparison with $Q_{D1} = 1.06 \pm 0.04$ eV and $Q_{D2} = 0.10 \pm 0.01$ eV in the symmetric Σ5 GB, respectively. Not only are all these values in excellent agreement individually, but the kink in the trend line corresponding to the transition from interstitial to vacancy-mediated diffusion in the symmetric boundary is also reflected in the GB migration data. We interpret the very close match of these kinetic data as strong evidence that GB migration is achieved via diffusion in the zero-velocity limit.

The diffusional characteristics of GB motion in the locked state help to explain the observed linear trend in Figs. 4(b) and 4(e) in the low driving force regime. In the locked state, GB atoms oscillate around their equilibrium positions and randomly hop back and forth across the interface due to thermal noise. This diffusional migration mechanism is the one envisioned by, e.g., Gottstein *et al.*,[7] and rate theory gives the velocity dependence on driving force as $v \propto \exp(P/kT)$, which can be reduced to the simple linear relationship of $v = MP$ as described in Eq. (1) when $P/kT \ll 1$ (e.g., at $T = 800$ K, $P = 0.005$ eV, $P/kT \approx 0.07 \ll 1$).

B. GB motion in the running state

The apparent linear regime of GB migration at large driving forces in Fig. 4 could indicate ballistic motion of GB atoms in the running state. In order to characterize the running state as well as the transition from locked to running, we simulate the migration of the inclined Σ5 GB under low driving forces from $P = 0.0001$ to 0.05 eV at 800 K using the AIRwalk method.

Figure 7(a) shows the time evolution of the GB displacement variance $\langle \sigma^2 \rangle$ among 12 independent simulations for each case. It is anticipated that for ballistic motion, the GB displacement variance will follow a quadratic dependence on time t,[52,53]

$$\langle \sigma^2(t) \rangle = \langle v^2 \rangle t^2, \qquad (13)$$

instead of a linear dependence for diffusional motion, as in Eq. (6). It is shown in Fig. 7(a) that when $P \geqslant 0.005$ eV, there are clear deviations from a simple linear dependence of $\langle \sigma^2 \rangle$ on t. A cleaner demonstration is provided by a plot of the square root of the GB displacement variance $\langle \sigma^2 \rangle$ as a function of time for $P = 0.01$ and 0.025 eV in Fig. 7(b), and fitted by Eq. (13). An excellent fit is found for both cases, with the coefficients
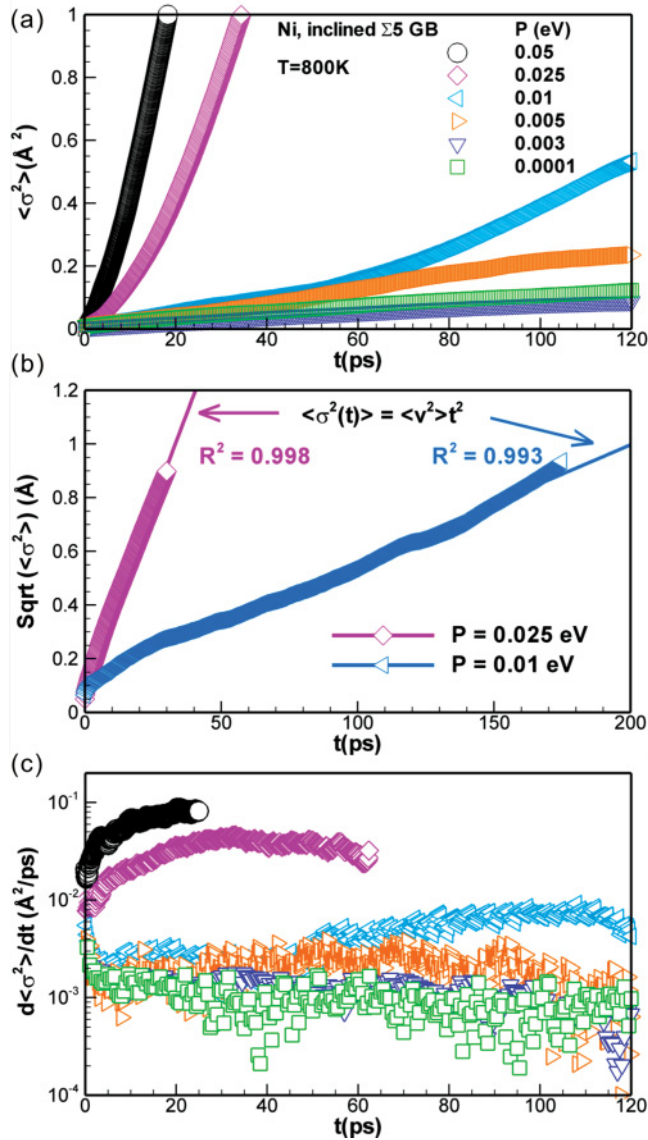
FIG. 7. (Color online) Time evolution of (a) the displacement variance $\langle \sigma^2 \rangle$ of the inclined Ni $\Sigma 5$ grain boundary under various driving forces and (b) the square root of $\langle \sigma^2 \rangle$ at $P = 0.01$ and 0.25 eV at 800 K; (c) the slope value of each data point on (a). The solid lines in (b) are linear fittings according to Eq. (13). Here, the driving force can be converted to Pa according to $1 \text{eV} \sim 1.47 \times 10^{10}$ Pa.

of determination R^2 greater than 0.99, thus confirming that in the high-bias, high-velocity regime, GB motion exhibits the characteristics of the ballistic running state.

Furthermore, the time evolution of the GB migration diffusion coefficient is plotted in Fig. 7(c) using the definition in Eq. (6). A transition of behavior is also clear in Fig 7(c); at low biases where diffusional migration is observed, D is a constant as expected, whereas when $P \geqslant 0.005$ eV and ballistic migration begins to set in, D is no longer a constant. We note that the critical driving force of $P = 0.005$ eV for the onset of this transition is in line with the rough estimation based on observations in Fig. 4 at 800 K. The time evolution of D

[see Fig. 7(c)], consequently, can be used as a signature to test whether GB motion is in the locked or running state.

C. Dependence of Q_m on P

It is now clear that the generally assumed linear relation between GB velocity v and the driving force P [see Eq. (1)] should only be applied for the conditions under which it was developed; for thermally activated GB migration where P is small enough that not only the trivial mathematical condition ($P \ll kT$) is fulfilled, but simultaneously the locked or diffusional state of GB migration is attained. Many extant MD studies on GB motion based on driven motion methods have extracted artificially high GB mobilities by using GB velocities ($\sim 10^1$ m/s) and driving forces in what we term the "transition" regime or even the ballistic regime.

In order to show how high simulated velocities and driving forces can lead to inaccurate measurement of GB mobilities and activation energies, we present in Fig. 8 an Arrhenius plot of GB mobility constructed by assuming the validity of Eq. (1) for both the symmetric and inclined $\Sigma 5$ GBs at all driving forces. In Fig. 8, the data points for $P = 0$ are "intrinsic" GB mobilities extracted from the AIRwalk method with zero net bias, and the data points for $P \sim 0$ are extracted from the AIRwalk method with driving forces in the locked/diffusional regime, which are determined by linearly fitting all the data points in the locked regime to Eq. (1) at each temperature.
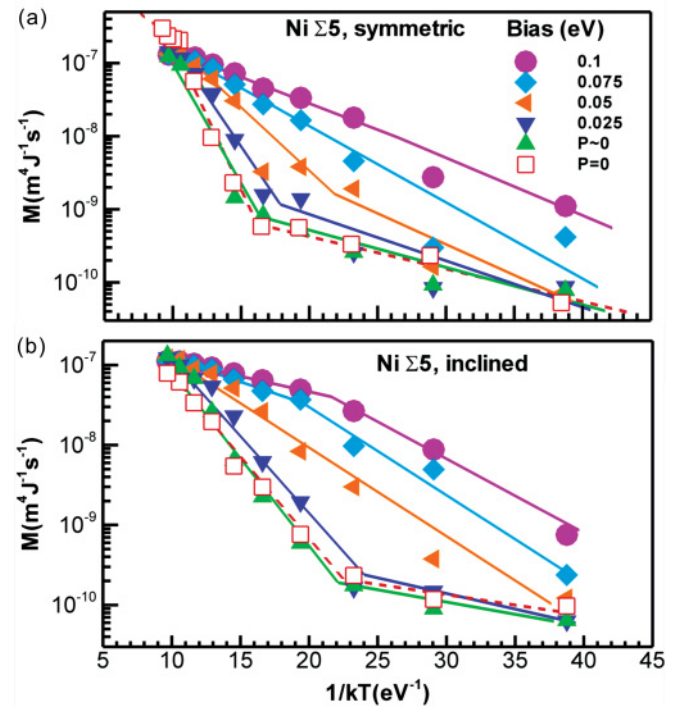
FIG. 8. (Color online) Arrhenius plot of mobility for the (a) symmetric and (b) inclined Ni $\Sigma 5$ grain boundary at various biases. The solid lines are added as guides for the eye, to show the slope changes. Here, the driving force can be converted to Pa according to $1 \text{eV} \sim 1.47 \times 10^{10}$ Pa.

Both Figs. 8(a) and 8(b) indicate that the measured GB mobilities agree well with the true, intrinsic values only when the driving force is sufficiently small; the deviation from the true mobility grows larger as the driving forces increase. As a result, the slopes from such Arrhenius plots yield only *apparent* activation energies when the driving forces are high. These apparent activation energies are not physical; they are significantly smaller than the intrinsic values in the high-temperature regime. For example, from Fig. 8, we observe that the analysis becomes flawed above about $T > 500$ K for the inclined $\Sigma 5$ GB, which is the typical temperature range in both experiments and prior MD simulations. Specifically, the measured activation energies for the inclined $\Sigma 5$ GB are $Q_m = 0.51$ eV when $P = 0$, $Q_m = 0.31$ eV when $P = 0.05$ eV, and $Q_m = 0.13$ eV when $P = 0.05$ eV.

While past MD studies have occasionally attributed the extracted lower activation energies as compared to experimental values to assumed impurities or other artifacts in the experimental data,[15,17,32] our simulations offer an alternative explanation. We propose that the discrepancy is more likely due to the high driving forces and high GB velocities in past MD simulations, which access the ballistic mode of GB motion; although such ballistic GB motion data exhibit a linear relationship between P and v, they cannot be validly analyzed using $v = MP$ [see Eq. (1)] to extract GB mobilities.

New evidence from this study also helps clarify the proposed mechanisms for GB motion at low-temperature regimes and the zero-driving-force limit in our preliminary report,[37] where we tentatively attributed the relatively low activation energy in that regime to a mechanism of transboundary atomic hopping. With more details from Fig. 6, this change of activation energy in different temperature regimes can now be associated with the transition between vacancy- and interstitial-dominated diffusional hoppings. As a corollary, the extracted "activation energy" of $Q_m = 0.125$ eV based on the driven motion method in that study[37] can now be interpreted as that required to trigger the transition from diffusional to ballistic motion for symmetric Ni $\Sigma 5$ GB at $T = 300$.

V. CONCLUSIONS

Atomistic simulations based on the AIRwalk method have been used to study the motion of both symmetric and inclined $\Sigma 5$ GBs over broad ranges of temperature and driving force. This investigation provides a complete map of the major modes of GB motion, and three major conclusions can be drawn: (i) although the velocity v of GB motion often appears to be a monotonic linear function of the applied driving force P, there are in fact two distinct linear regimes as well as a transition regime in between. The transition is extremely broad at low temperatures and narrow at high temperatures. (ii) The two linear P-v regimes correspond to dramatically different kinetic modes of GB motion: the linear regime at low driving forces has the characteristic behavior of diffusional GB motion in the locked state, while the linear regime at high driving forces corresponds to ballistic GB motion in the running state. The transition from diffusive to ballistic GB motions can be identified by tracking the GB displacement variance $\langle \sigma^2(t) \rangle$ among a large number of independent simulations; $\langle \sigma^2(t) \rangle$ changes from linear for diffusional motion to quadratic for ballistic motion. (iii) GB mobility extracted from the transition or ballistic regimes by assuming $v = MP$ will lead to apparent activation energies that are significantly different from the true value (and generally lower). This artifact may be present in many extant MD simulation works on GB migration, and provides an alternate explanation for the mismatch between reported activation energies from atomistic simulations and experiments.

[*]schuh@mit.edu

[1]A. P. Sutton, Ceramic Transactions **118**, 3 (2000).

[2]R. W. Balluffi, I. Majid, and P. D. Bristowe, *Characterization of the Structure and Chemistry of Defects in Materials*, edited by B. C. Larson, M. Ruhle, and D. N. Seidman, MRS Symposia Proceedings No. 138 (Materials Research Society, Pittsburgh, PA, 1989), p. 457.

[3]R. W. Balluffi and A. P. Sutton, Mater. Sci. Forum. **207**, 1 (1996).

[4]A. P. Sutton and R. W. Balluffi, *Interfaces in Cystalline Materials* (Clarendon Press, Oxford University, Oxford New York, 1995).

[5]M. Hillert, Acta Metall. **13**, 227 (1965).

[6]T. J. Rupert and C. A. Schuh, Acta Mater. **58**, 4137 (2010).

[7]G. Gottstein and L. S. Shvindlerman, *Grain Boundary Migration in Metals: Thermodynamics, Kinetics, Applications* (CRC Press, Boca Raton, Fl., 1999).

[8]A. J. Detor and C. A. Schuh, J. Mater. Res. **22**, 3233 (2007).

[9]D. S. Gianola, S. Van Petegem, M. Legros, S. Brandstetter, H. Van Swygenhoven, and K. J. Hemker, Acta Mater. **54**, 2253 (2006).

[10]T. J. Rupert, D. S. Gianola, Y. Gan, and K. J. Hemker, Science **326**, 1686 (2009).

[11]D. L. Olmsted, E. A. Holm, and S. M. Foiles, Acta Mater. **57**, 3704 (2009).

[12]H. Zhang, P. Kalvapalle, and J. F. Douglas, Soft Matter **6**, 5944 (2010).

[13]A. I. Dmitriev, A. Y. Nikonov, and S. G. Psakhie, Tech. Phys. Lett. **36**, 786 (2010).

[14]E. A. Holm and S. M. Foiles, Science **328**, 1138 (2010).

[15]H. Zhang, M. I. Mendelev, and D. J. Srolovitz, Acta Mater. **52**, 2569 (2004).

[16]H. Zhang, N. Upmanyu, and D. J. Srolovitz, Acta Mater. **53**, 79 (2005).

[17]H. Zhang, M. I. Mendelev, and D. J. Srolovitz, Scr. Mater. **52**, 1193 (2005).

[18] H. Zhang, D. X. Du, D. J. Srolovitz, and M. I. Mendelev, Appl. Phys. Lett. **88**, 121927 (2006).

[19] A. Suzuki and Y. Mishin, New Frontiers of Processing and Engineering in Advanced Materials **502**, 157 (2005).

[20] J. W. Cahn, Y. Mishin, and A. Suzuki, Acta Mater. **54**, 4953 (2006).

[21] V. A. Ivanov and Y. Mishin, Phys. Rev. B **78**, 064106 (2008).

[22] Y. Mishin, A. Suzuki, B. P. Uberuaga, and A. F. Voter, Phys. Rev. B **75**, 224101 (2007).

[23] K. G. F. Janssens, D. Olmsted, E. A. Holm, S. M. Foiles, S. J. Plimpton, and P. M. Derlet, Nat. Mater. **5**, 124 (2006).

[24] J. Monk and D. Farkas, Phys. Rev. B **75**, 045414 (2007).

[25] D. Farkas, S. Mohanty, and J. Monk, Mater. Sci. Eng. A **493**, 33 (2008).

[26] D. Farkas, A. Froseth, and H. Van Swygenhoven, Scripta Materialia **55**, 695 (2006).

[27] F. Sansoz and V. Dupont, Appl. Phys. Lett. **89**, 111901 (2006).

[28] S. M. Foiles and J. J. Hoyt, Solid-Solid Phase Transformations in Inorganic Materials **1**, 615 (2005).

[29] J. J. Hoyt, Z. T. Trautt, and M. Upmanyu, Mathematics and Computers in Simulation **80**, 1382 (2010).

[30] M. Upmanyu, D. J. Srolovitz, A. E. Lobkovsky, J. A. Warren, and W. C. Carter, Acta Mater. **54**, 1707 (2006).

[31] Z. T. Trautt, M. Upmanyu, and A. Karma, Science **314**, 632 (2006).

[32] B. Schonfelder, P. Keblinski, D. Wolf, and S. R. Phillpot, Mater. Sci. Forum **294-296**, 9 (1998).

[33] B. Schonfelder, D. Wolf, S. R. Phillpot, and M. Furtkamp, Interface Sci. **5**, 245 (1997).

[34] V. Yamakov, D. Moldovan, K. Rastogi, and D. Wolf, Acta Mater. **54**, 4053 (2006).

[35] D. L. Olmsted, S. M. Foiles, and E. A. Holm, Scr. Mater. **57**, 1161 (2007).

[36] S. M. Foiles and J. J. Hoyt, Acta Mater. **54**, 3351 (2006).

[37] C. A. Deng and C. A. Schuh, Phys. Rev. Lett. **106**, 045503 (2011).

[38] G. J. Ackland and A. P. Jones, Phys. Rev. B **73**, 054104 (2006).

[39] S. Plimpton, J. Comput. Phys. **117**, 1 (1995).

[40] G. J. Ackland, G. Tichy, V. Vitek, and M. W. Finnis, Philos. Mag. A **56**, 735 (1987).

[41] S. Nose, J. Chem. Phys. **81**, 511 (1984).

[42] W. G. Hoover, Phys. Rev. A **31**, 1695 (1985).

[43] M. C. Payne, P. D. Bristowe, and J. D. Joannopoulos, Phys. Rev. Lett. **58**, 1348 (1987).

[44] C. Schmidt, M. W. Finnis, F. Ernst, and V. Vitek, Philos. Mag. A **77**, 1161 (1998).

[45] K. Lindenberg, A. M. Lacasta, J. M. Sancho, and A. H. Romero, New J. Phys. **7**, 29 (2005).

[46] G. Costantini and F. Marchesoni, Europhys. Lett. **48**, 491 (1999).

[47] G. Gottstein, U. Czubayko, D. A. Molodov, L. S. Shvindlerman, and W. Wunderlich, Mater. Sci. Forum. **204**, 99 (1996).

[48] G. Gottstein, D. A. Molodov, L. S. Shvindlerman, and M. Winning, *Materials for the Third Millennium*, edited by K. Ray *et al.* (Oxford & IBH Publ., New Delhi, India, 2001), p. 237.

[49] G. Gottstein, L. S. Shvindlerman, D. A. Molodov, and U. Czubayko, *Dynamics of Crystal Surfaces and Interfaces*, edited by P. M. Duxbury and T. J. Pence (Plenum Press, NY, 1997), p. 109.

[50] C. L. Liu and S. J. Plimpton, Phys. Rev. B **51**, 4523 (1995).

[51] A. Suzuki and Y. Mishin, J. Mater. Sci. **40**, 3155 (2005).

[52] T. C. Li, S. Kheifets, D. Medellin, and M. G. Raizen, Science **328**, 1673 (2010).

[53] P. N. Pusey, Science **332**, 802 (2011).